nature sustainability

Supplementary information

https://doi.org/10.1038/s41893-024-01431-6

Low-cost iron trichloride cathode for all-solid-state lithium-ion batteries

In the format provided by the authors and unedited

Table of Contents

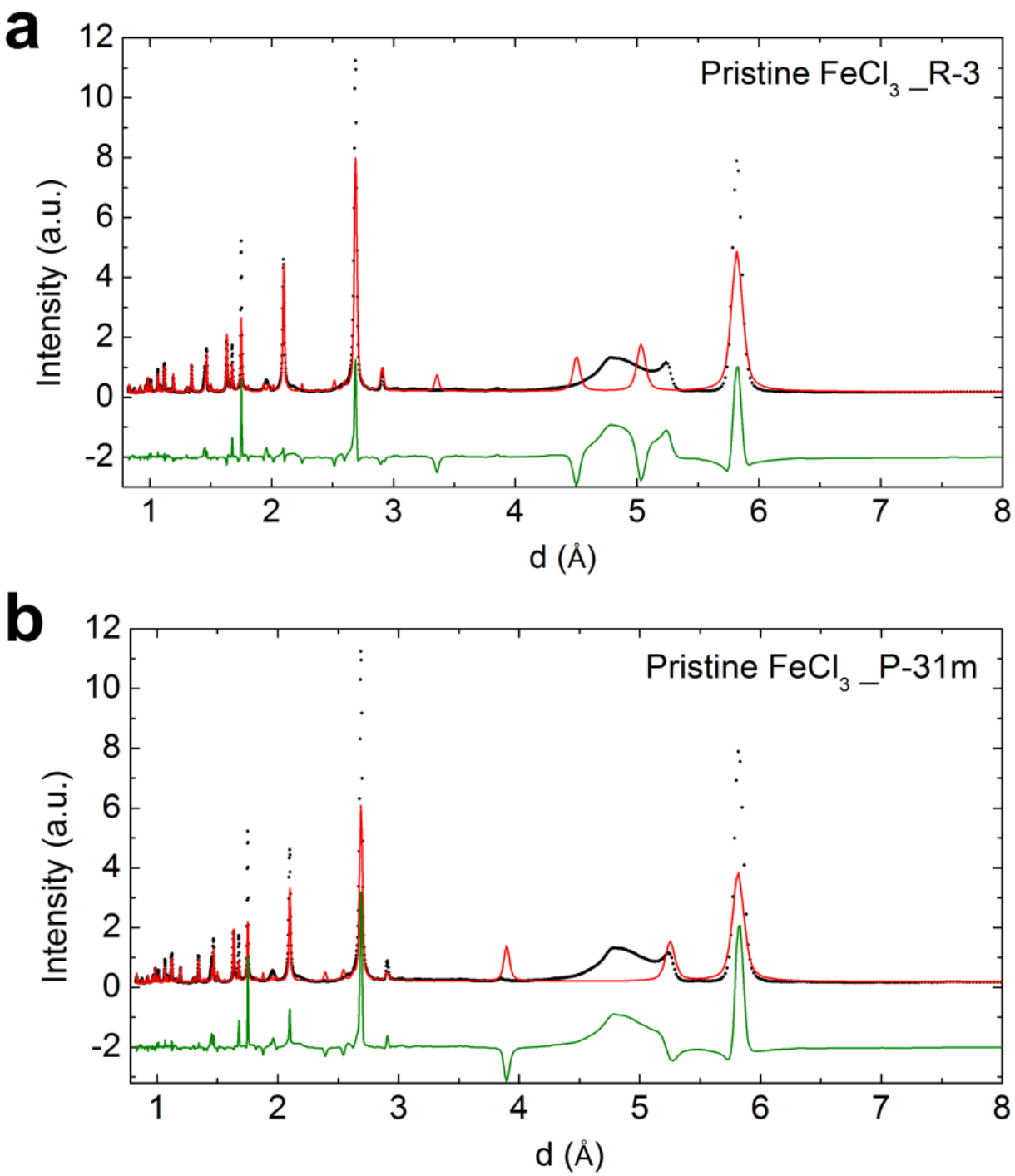

Supplementary Figure 1. Rietveld refinements against synchrotron diffraction pattern of pristine $FeCl_3$ using two structure models with different stacking sequences of the honeycomb-ordered Fe-vacancy layers along *c*-axis direction ((a) S.G. $R\bar{3}$ and (b) S.G. $P\bar{3}1m$, respectively).

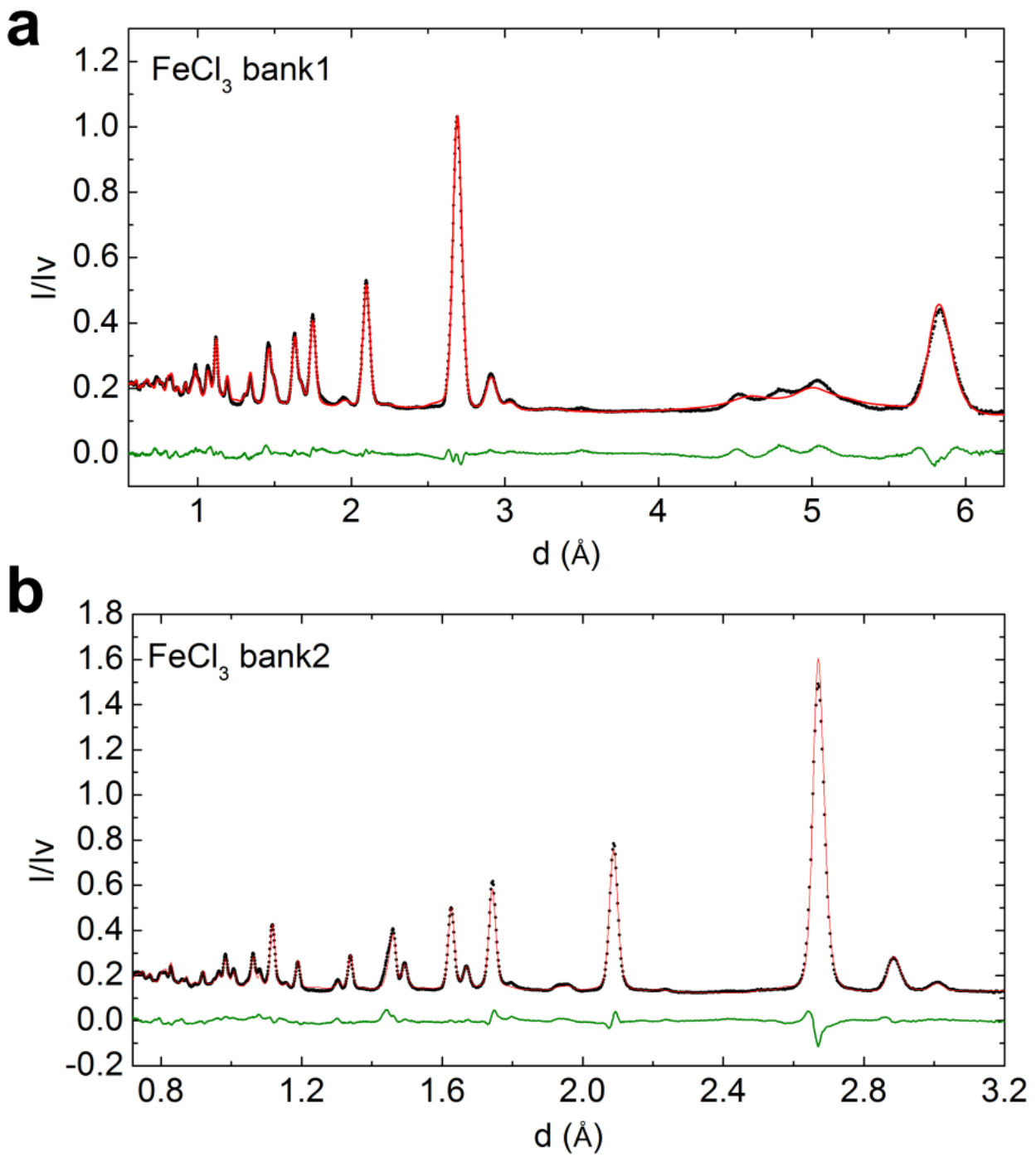

Supplementary Figure 2. Rietveld refinement against neutron diffraction pattern of pristine $FeCl_3$ with using the stacking-disorder model. (Rwp = 4.85%, Gof = 8.05)

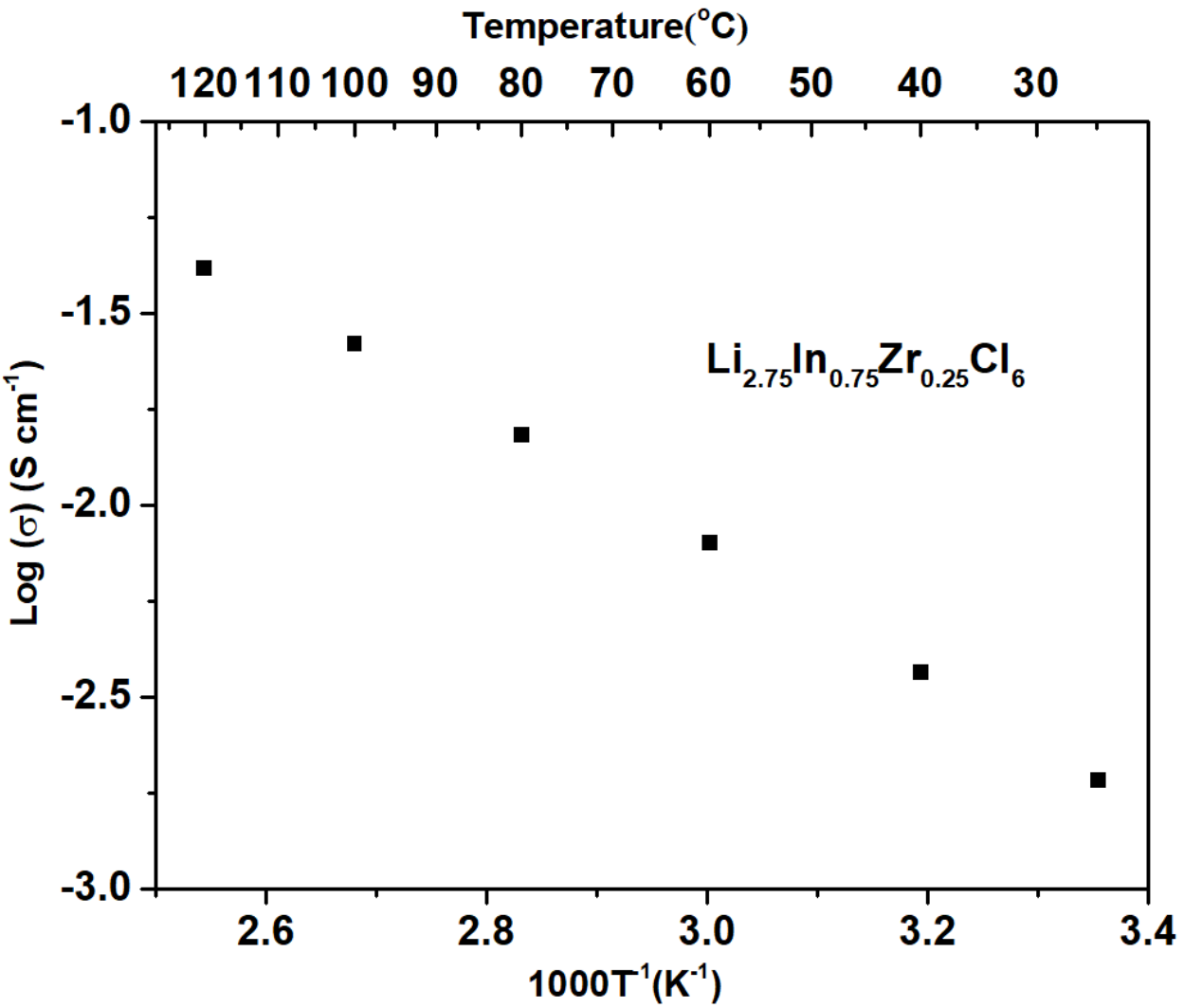

Supplementary Figure 3. Arrhenius plots of ball-milled $Li_{2.75}In_{0.75}Zr_{0.25}Cl_6$. The cold-pressed pellet exhibits an ionic conductivity of 1.9 mS cm^{-1} at 25 °C with an activation energy of 0.32 eV.

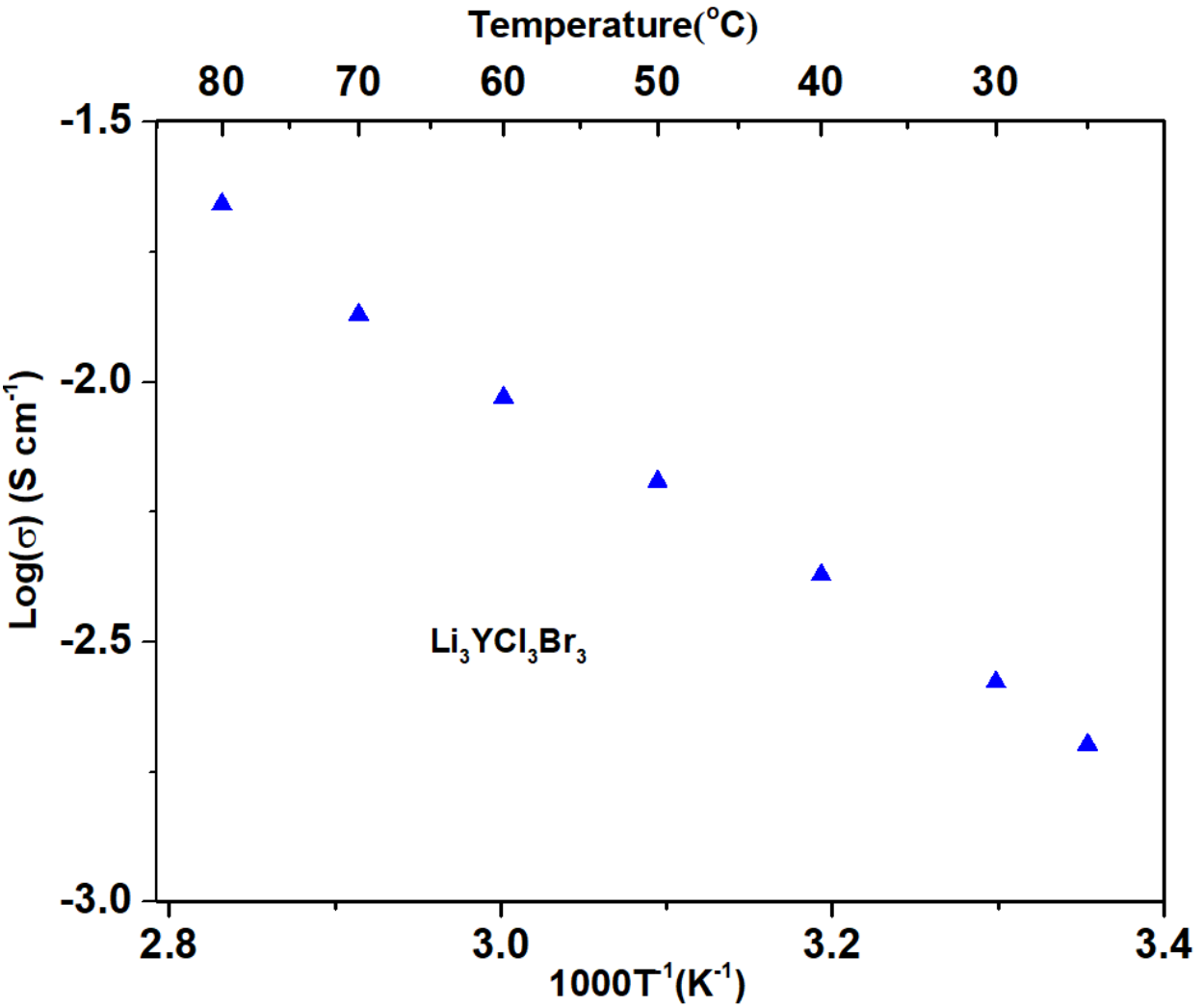

Supplementary Figure 4. Arrhenius plots of LYCB. The cold-pressed pellet exhibits an ionic conductivity of 2.0 mS cm^{-1} at 25 °C with an activation energy of 0.41 eV.

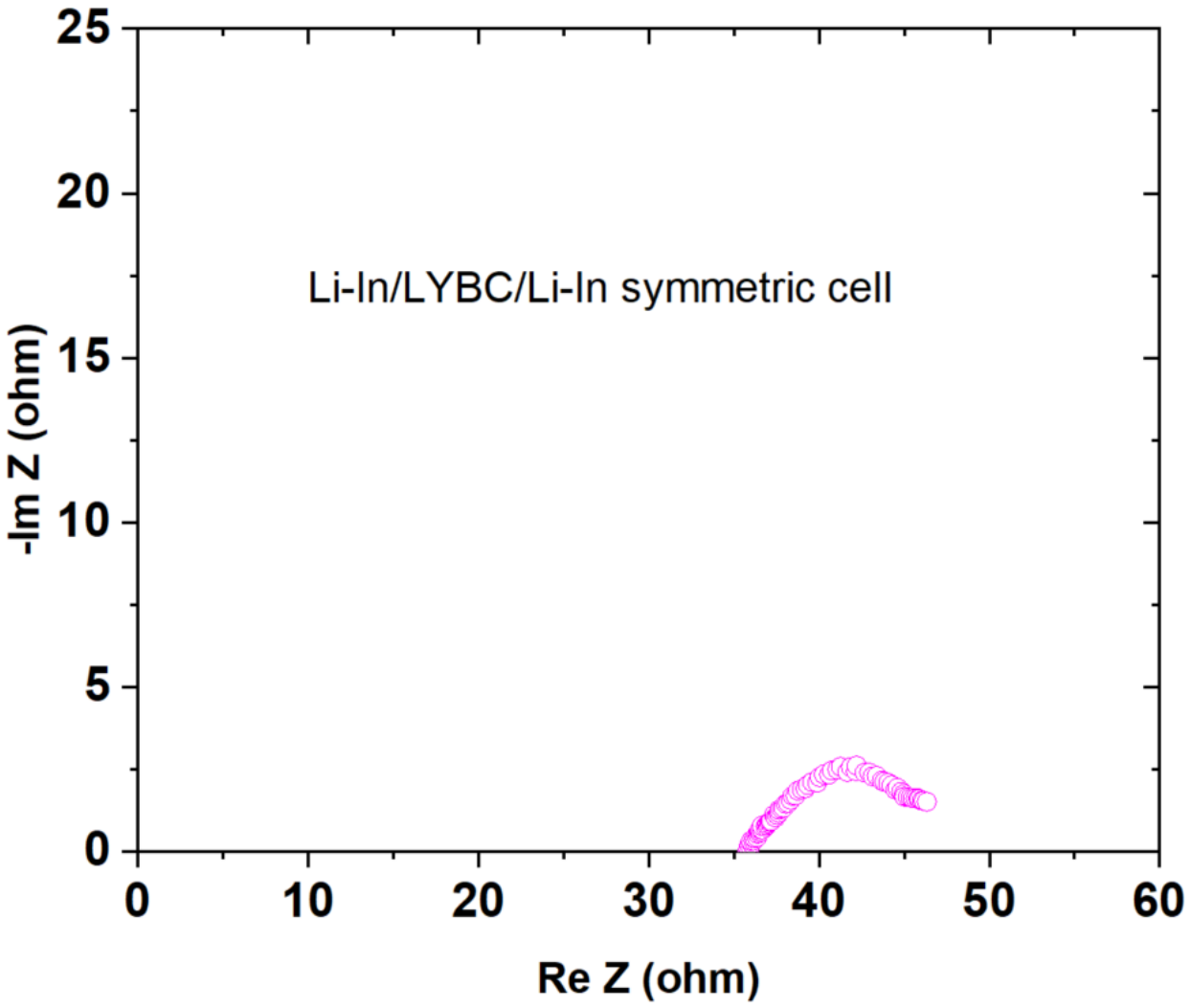

Supplementary Figure 5. Nyquist plot of the Li-In/LYBC/Li-In symmetric cell.

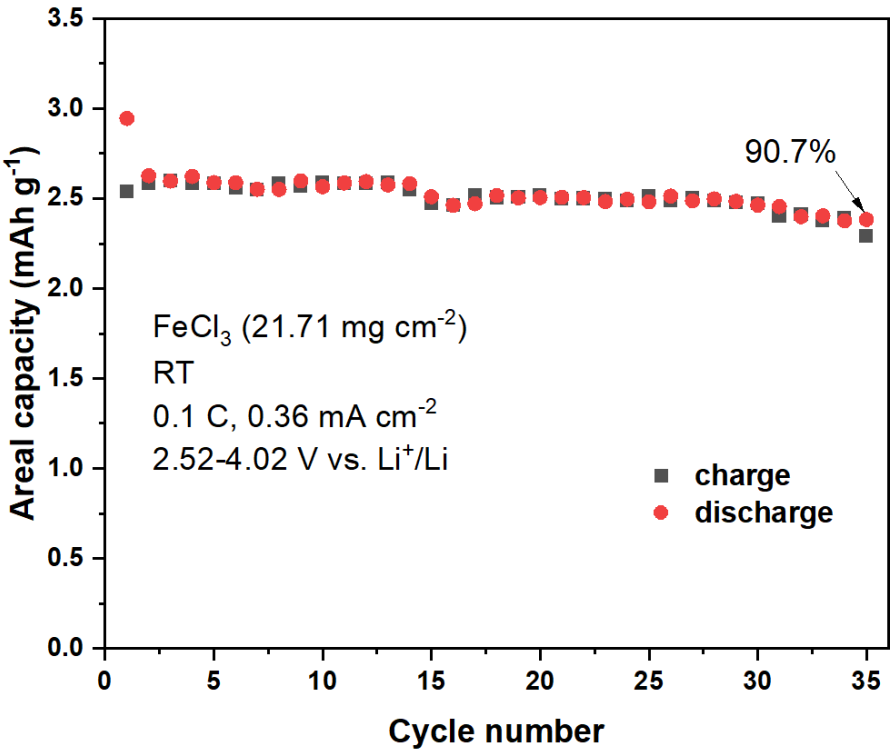

Supplementary Figure 6. $FeCl_3$ cell cycled at 0.1 C between 2.52 and 4.02 V vs. Li^+/Li at room temperature. The mass loading of $FeCl_3$ is 21.71 $mg \cdot cm^{-2}$.

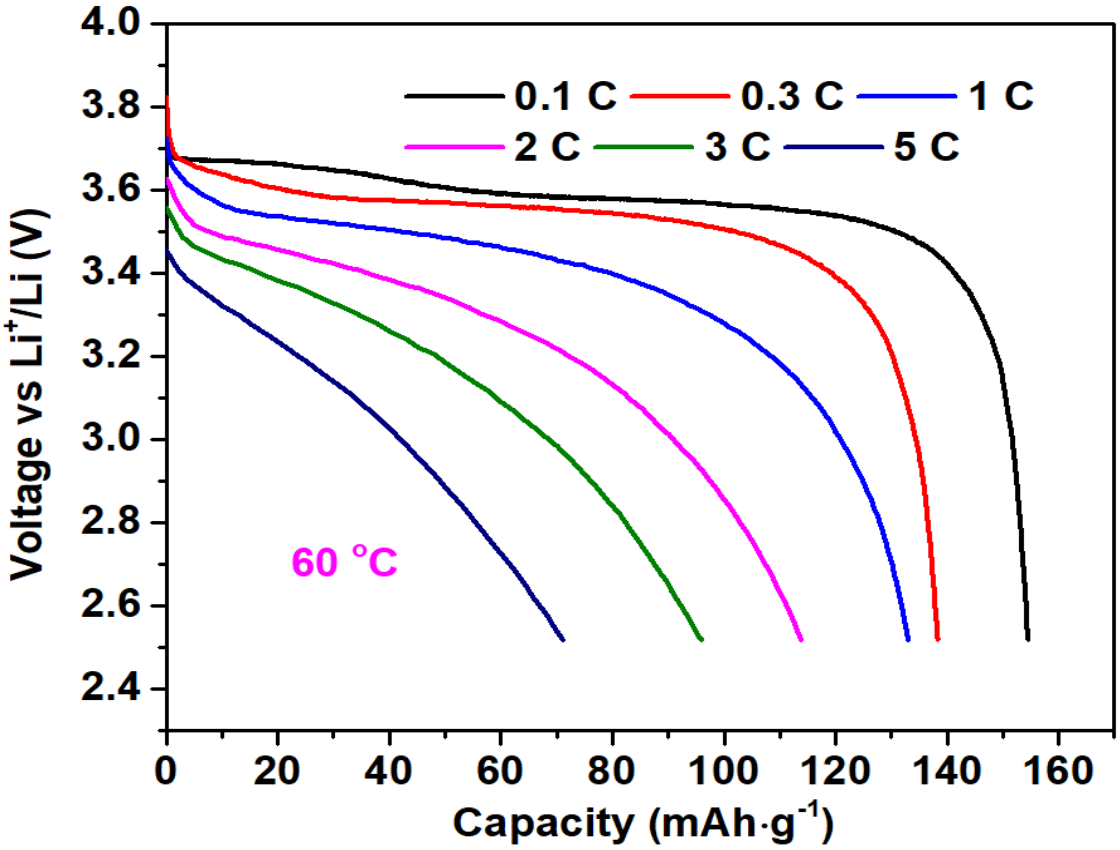

Supplementary Figure 7. Rate performance of $FeCl_3$ SSLIB at 60 ^{o}C. The charge/discharge voltage range is between 2.52 to 4.12 V vs. Li^+/Li.

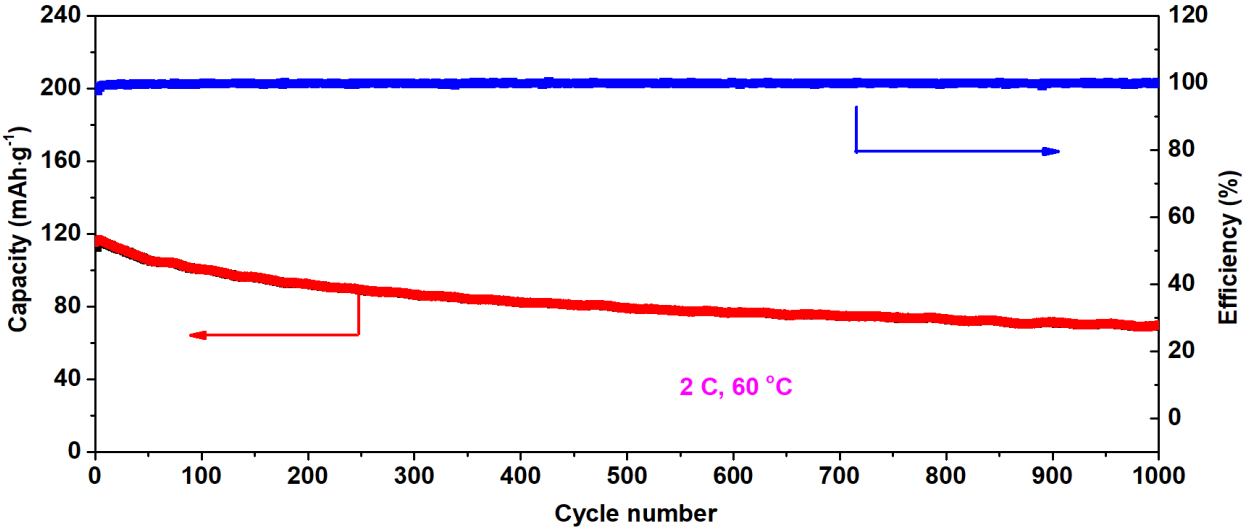

Supplementary Figure 8. Long-term cycling performance of $FeCl_3$ SSLIB under 2C rate at 60 ^oC. The charge/discharge voltage range is between 2.52 to 4.12 V vs. Li^+/Li.

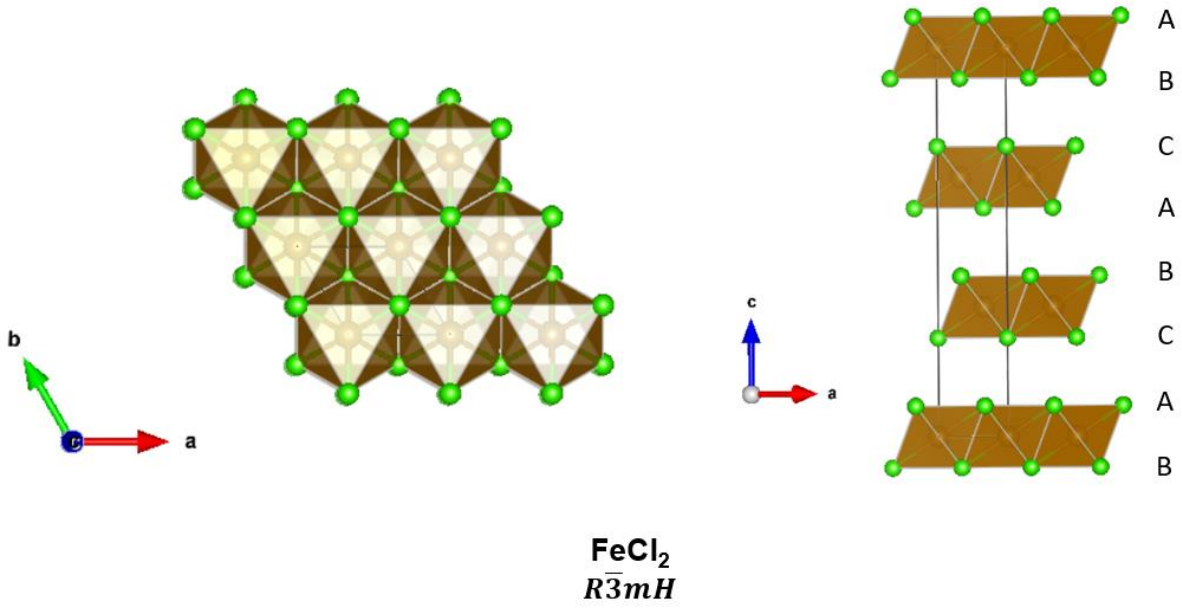

Supplementary Figure 9. Crystal structure of $FeCl_2$.

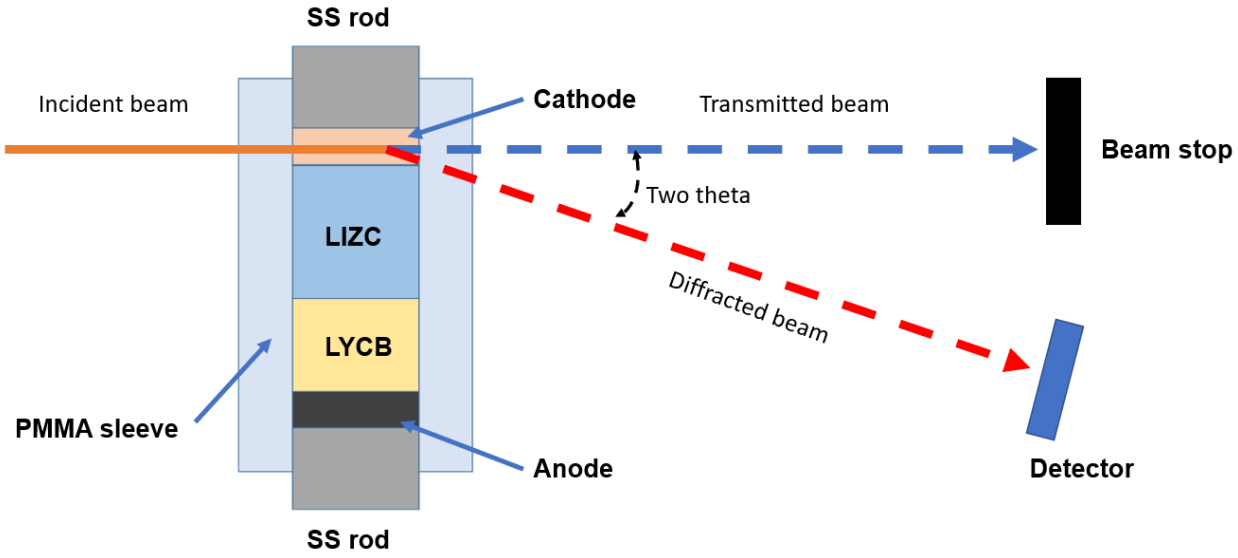

Supplementary Figure 10. Schematic demonstration of operando EDXRD set-up.

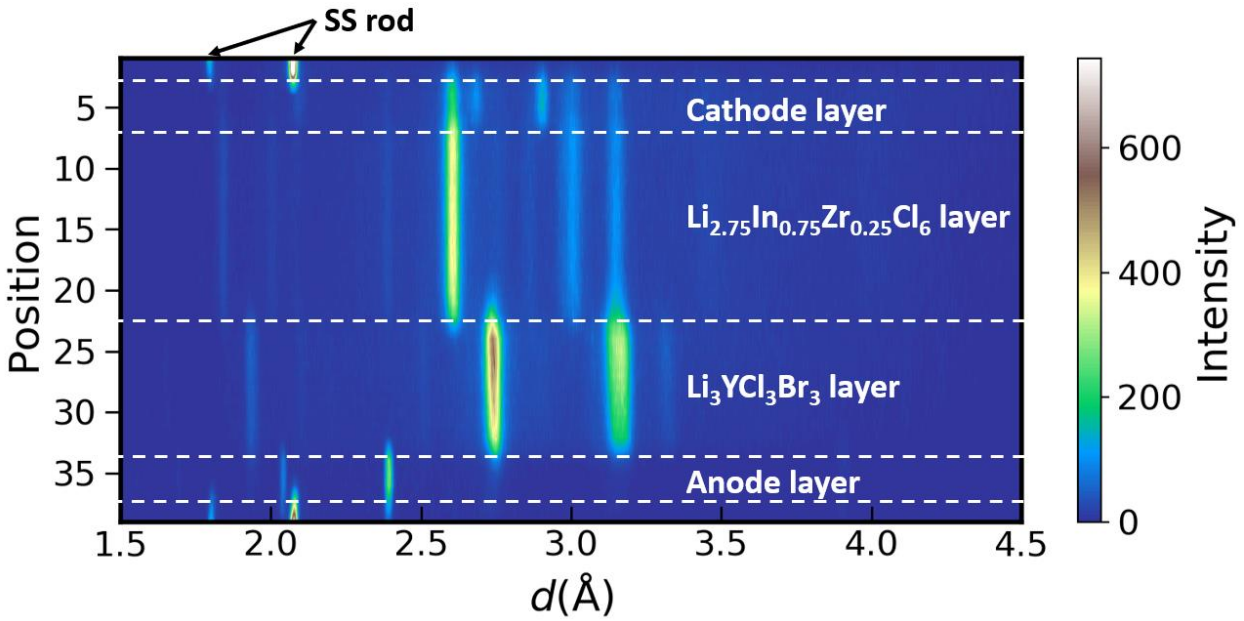

Supplementary Figure 11. EDXRD contour map between 1.5 and 4.5 Å of the $FeCl_3$ cell before cycling. EDXRD data were collected for 39 layers (20 μm per scan) to obtain full scans of the $FeCl_3$ cell before discharging/charging processes. The reflections from $FeCl_3$ are observable in layer 2 to 7.

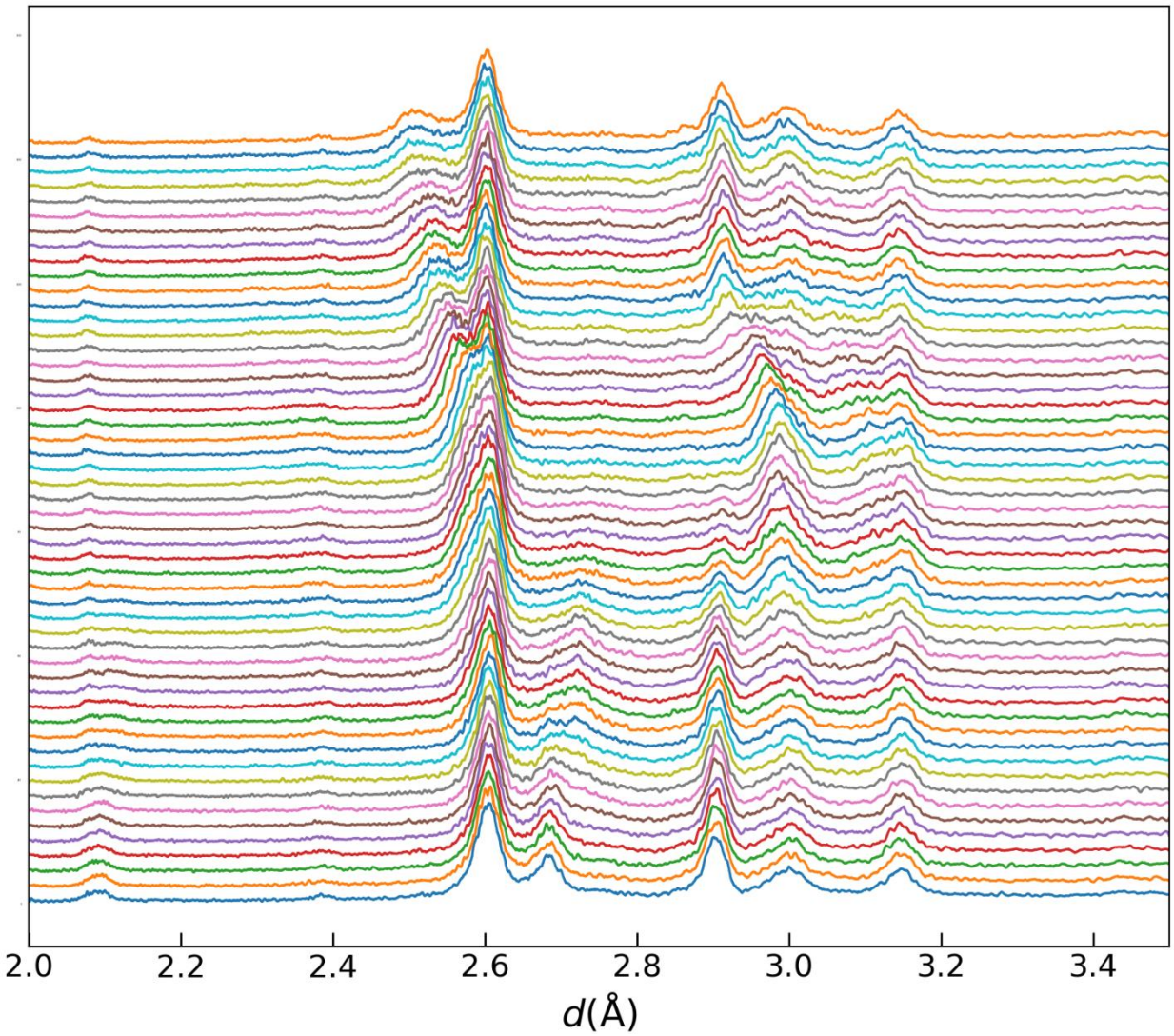

Supplementary Figure 12. Energy dispersive diffraction data between 2 and 3.5 Å in layer 5 during initial discharge/charge process.

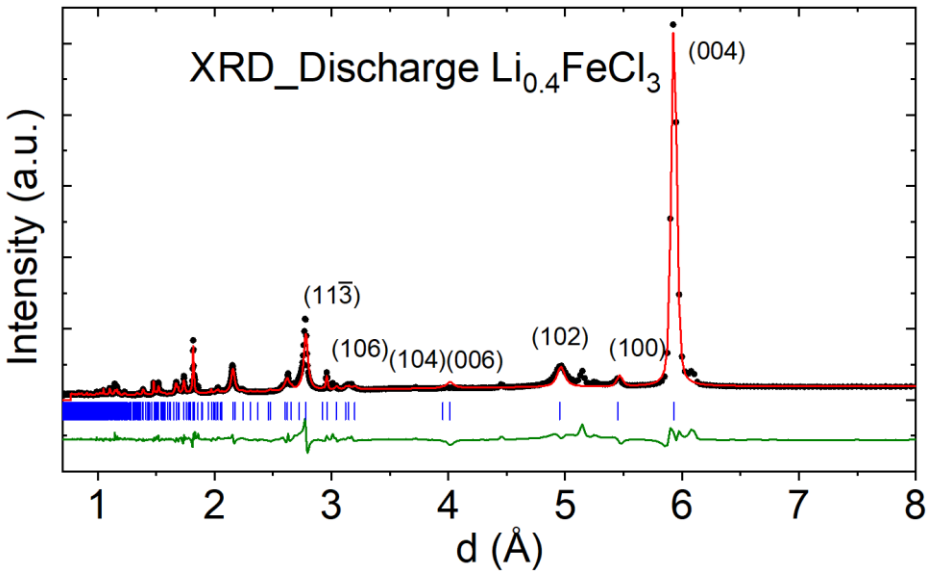

Supplementary Figure 13. Rietveld refinement against discharged $Li_{0.4}FeCl_3$ synchrotron powder diffraction pattern. The Bragg peaks can be indexed using space group $P6_3cm$. Diffraction data are shown in black dots, calculated pattern in red curve and difference curve in olive. The Bragg reflection positions are shown in blue marks.

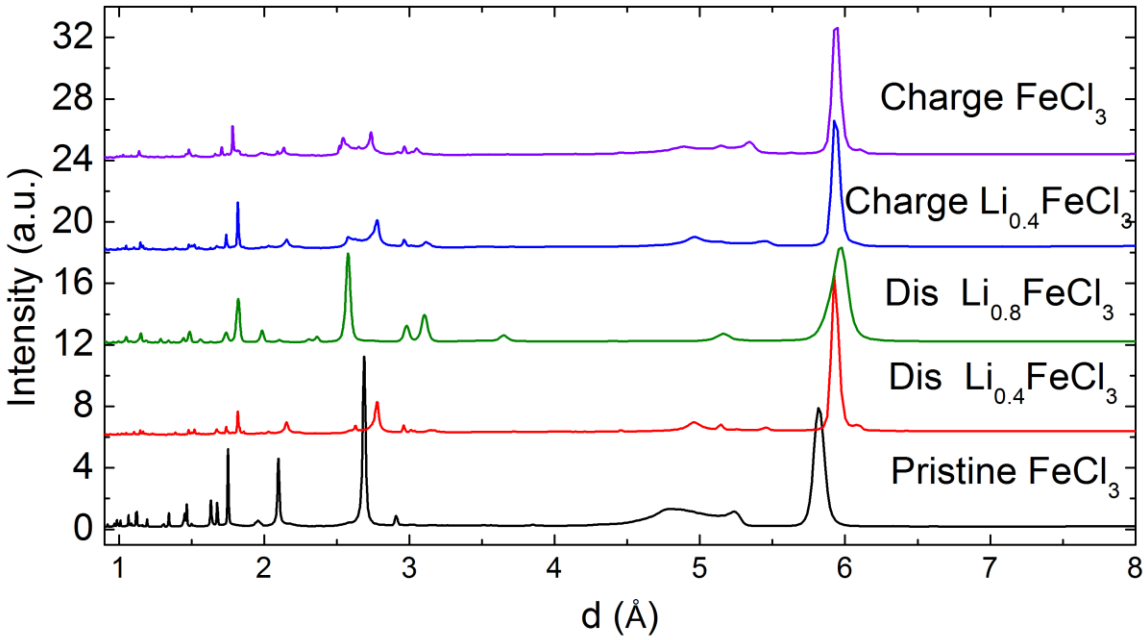

Supplementary Figure 14. Ex situ XRD data of Li_xFeCl_3 during the initial charge and discharge. It can be seen that both *ab*-plane and *c*-axis expand after intercalating ~0.4 Li^+, as evidenced from the shift of the diffraction peaks to higher d-spacings. The broad diffuse scattering peak (Warren peak) around 5 Å splits into multiple sharper diffraction peaks, indicating the change of in-plane Fe-vacancy honeycomb ordering due to partial Fe migration. These superlattice peaks disappear and merge into a single peak during further lithiation to $Li_{0.8}FeCl_4$. The deeply discharged sample ($Li_{0.8}FeCl_3$) adopts a distorted spinel structure with cation vacancies predominately occupy the tetrahedral sites. It is worth noting the transition between $Li_{0.4}FeCl_3$ and $Li_{0.8}FeCl_3$ is fully reversible, but removing Li^+ from charged $Li_{0.4}FeCl_3$ results in the charged $FeCl_3$ which adopts a different structure than the pristine $FeCl_3$.

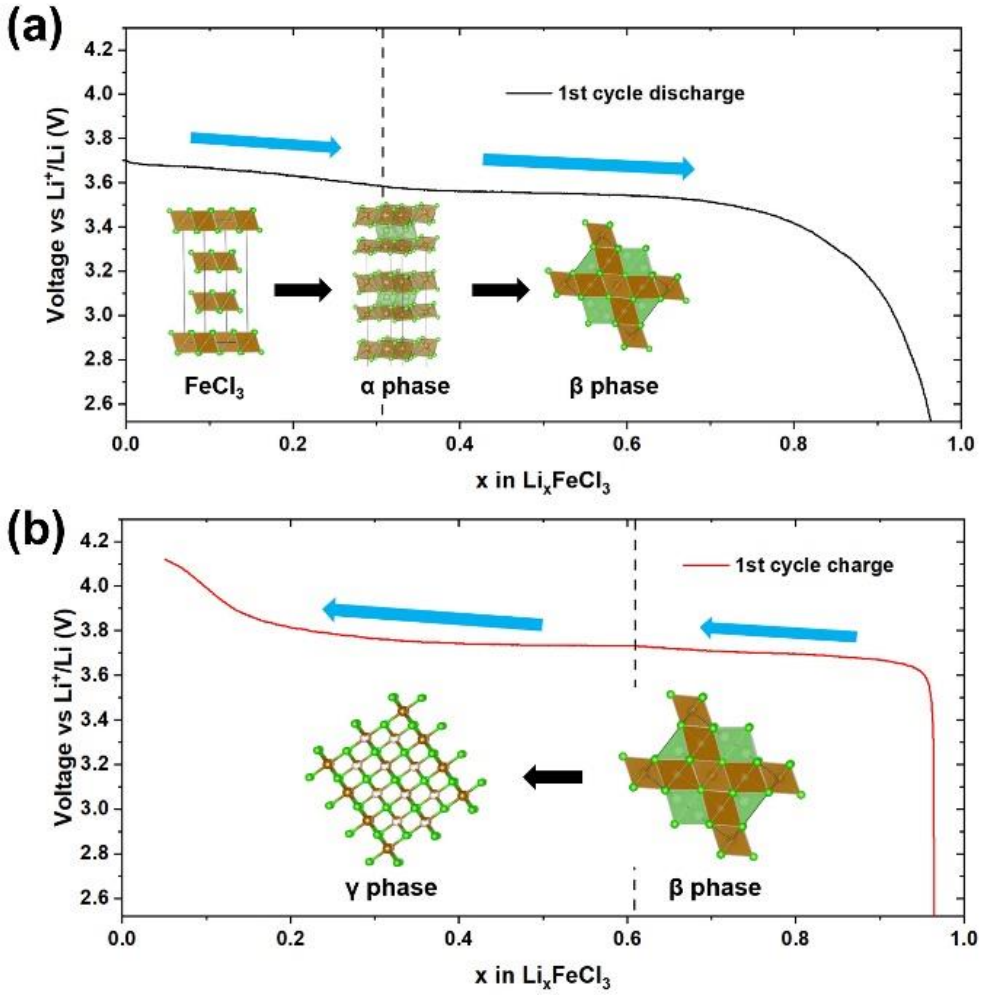

Supplementary Figure 15. Structure evolution diagram of $FeCl_3$ in solid cells in the charge-discharge process.

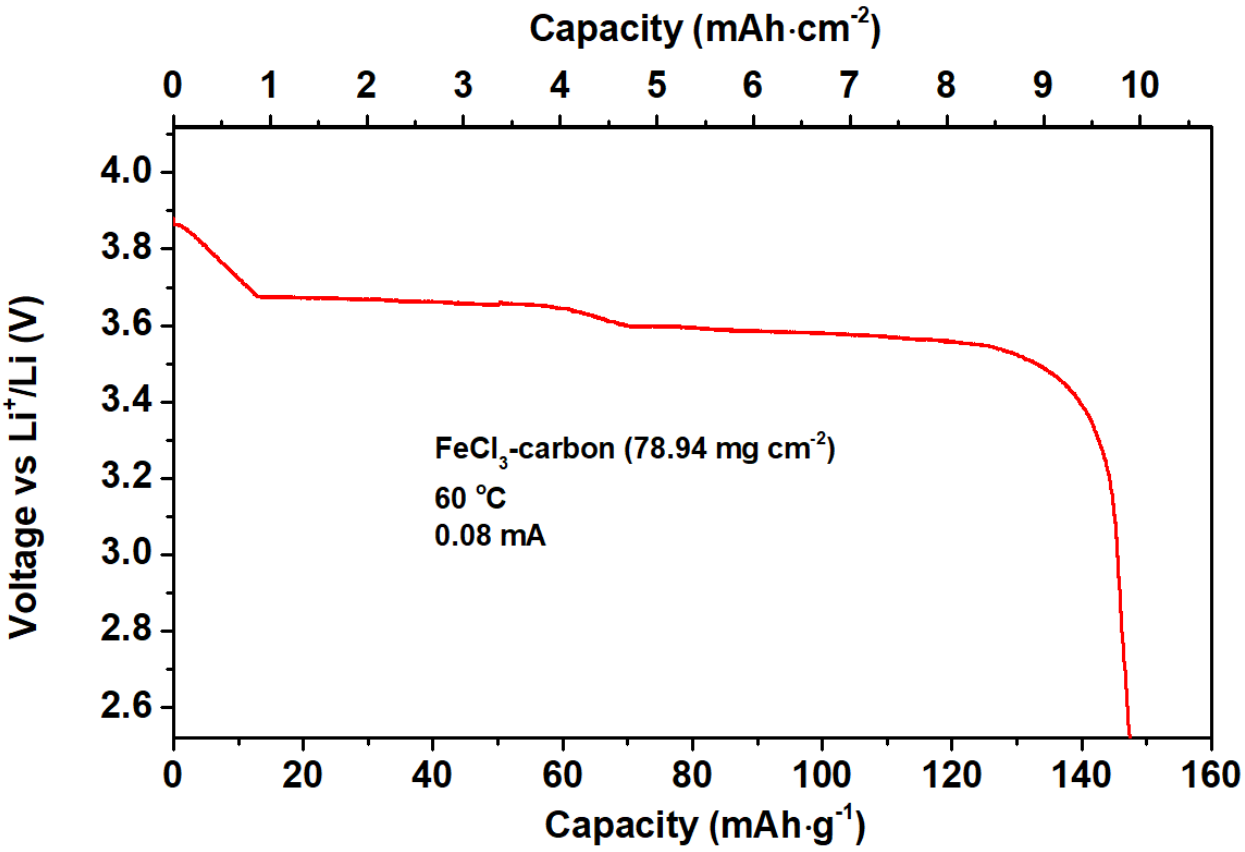

Supplementary Figure 16. Discharge profile of $FeCl_3$-carbon high-loading solid cell. $FeCl_3$ and carbon are mixed in a weight ratio of 85:15 without adding extra electrolyte. The cell has a high loading of 78.94 mg cm^{-2} and exhibits an areal capacity of 9.9 mAh cm^{-2}.

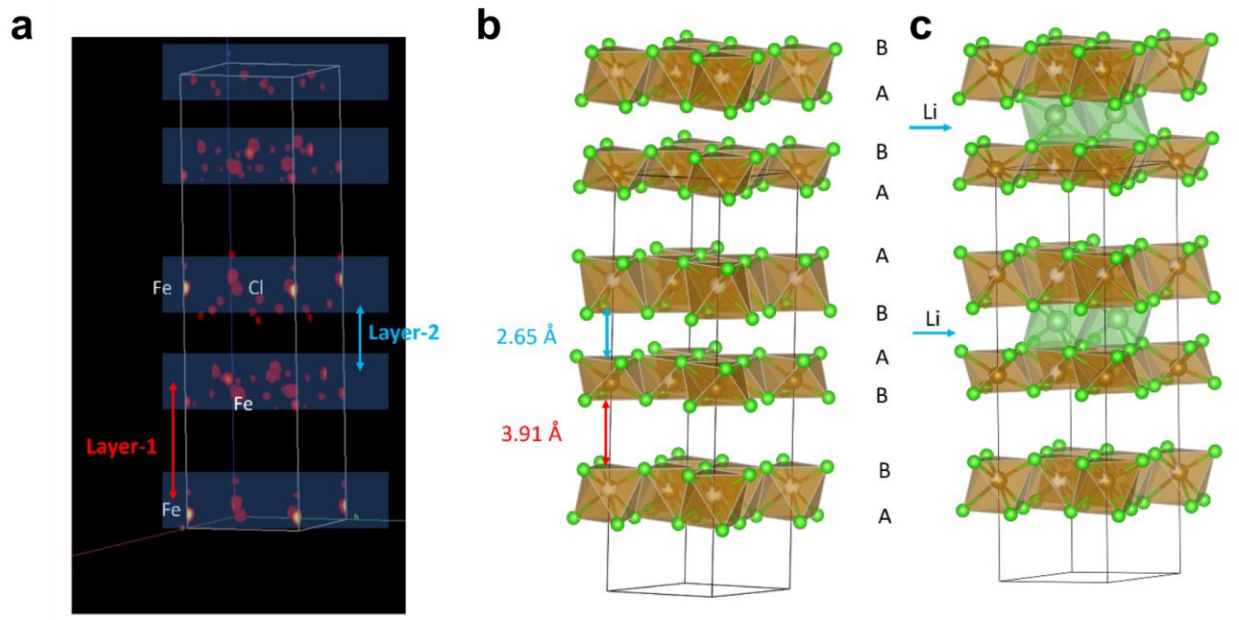

Supplementary Figure 17. (a) Major electron densities identified after successful charge flipping using the modular of structure factors obtained from Le Bail fit of XRD data. (b) Refined average crystal structure of first discharged $Li_{0.4}FeCl_3$ from Rietveld refinement without Li^+. (c) Refined crystal structure of $Li_{0.4}FeCl_3$ with plausible Li sites, highlighting that the intercalated Li^+ is likely reside on the octahedra sites between the AB stacked Fe-Cl layers.

Note: Ab initio structure solution was performed using charge charge-flipping algorithm to obtain the major electron density distribution. The major electron densities are distributed in four separate layers in the unit cell, with two different interlayer distances. The refined which indeed shows two distinct interlayer spacings, with the smaller interlayer spacing (~2.65 Å) residing between two AB stacked Cl layers, while the larger interlayer spacing (~3.91 Å) between two AA stacked Cl layers.

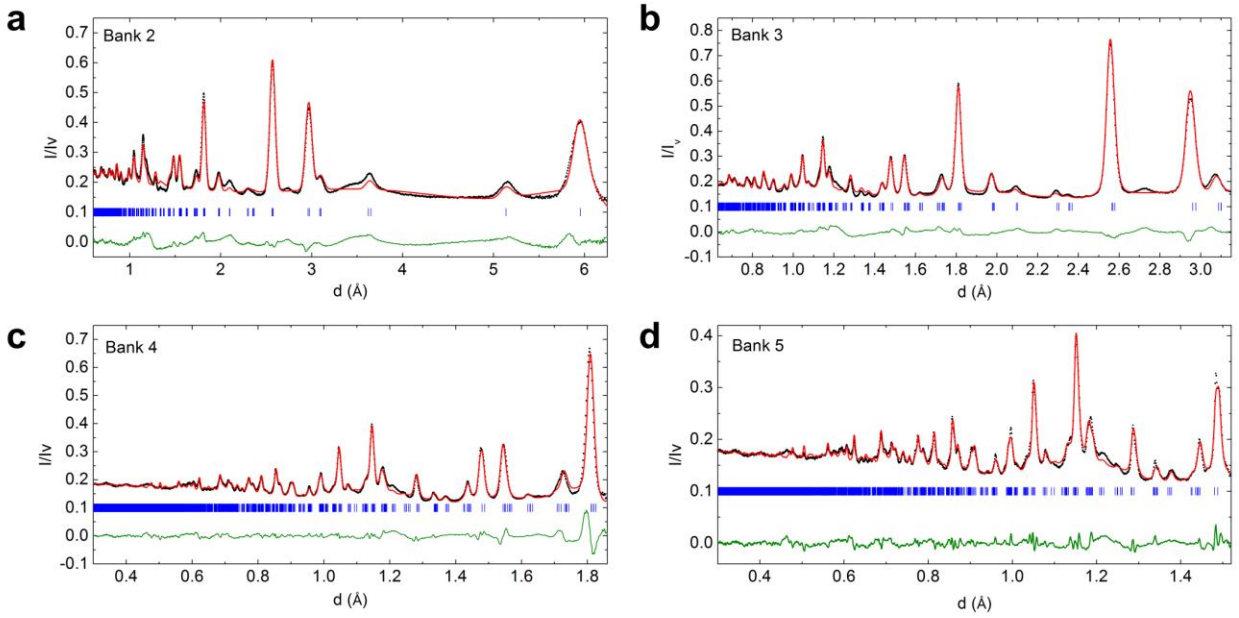

Supplementary Figure 18. Rietveld refinement of discharged $Li_{0.74}FeCl_3$ against neutron diffraction data collected at different banks. Experiment data are shown in black dots, calculated pattern in red curve and difference curve in olive. The Bragg reflections are shown in blue tick marks. The broad diffraction peaks around 3.5, 2.7 and 2 Å are from the carbon black additive.

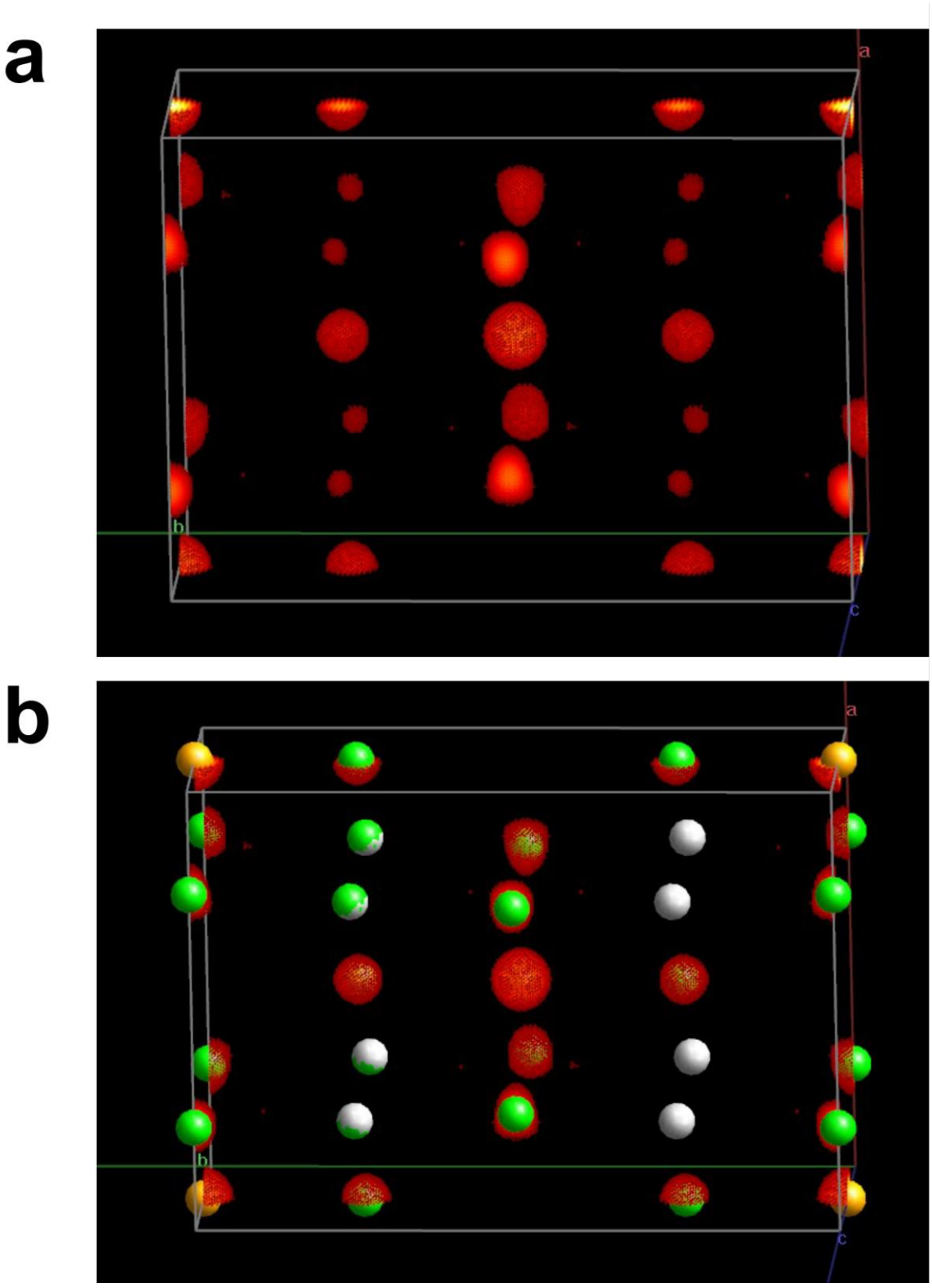

Supplementary Figure 19. Ab initio structure solution of $Li_{0.8}FeCl_3$ (from XRD) using the charge flipping algorithm. The majority of the electron density of cations are found to locate on the octahedral sites.

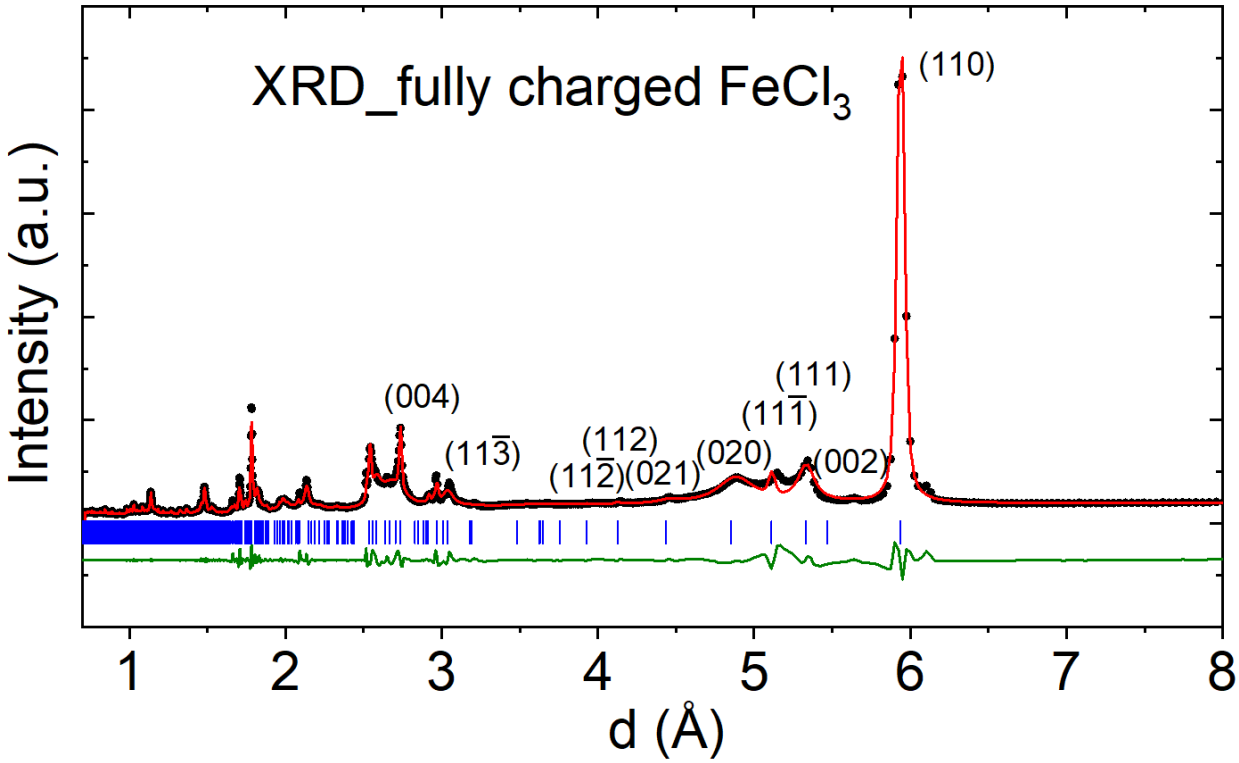

Supplementary Figure 20. Le bail fit result of fully charged $FeCl_3$ against synchrotron powder diffraction data (λ = 0.1875 Å). The Bragg peaks can be indexed using a space group *C2/m*. Diffraction data are shown in black dots, calculated pattern in red curve and difference curve in olive. The Bragg reflection positions are shown in blue marks.

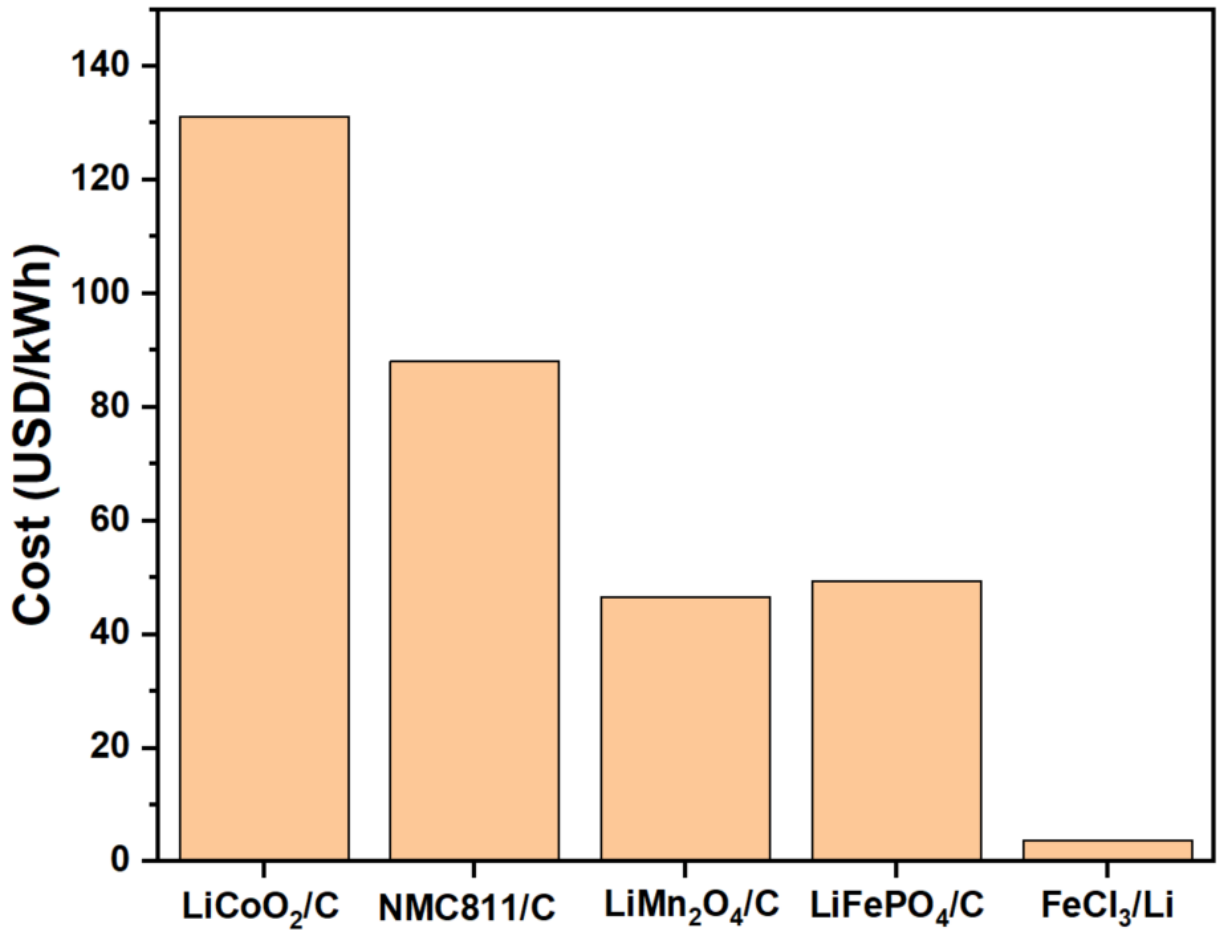

Supplementary Figure 21. Calculated cost of cathode/anode pairs per kWh.

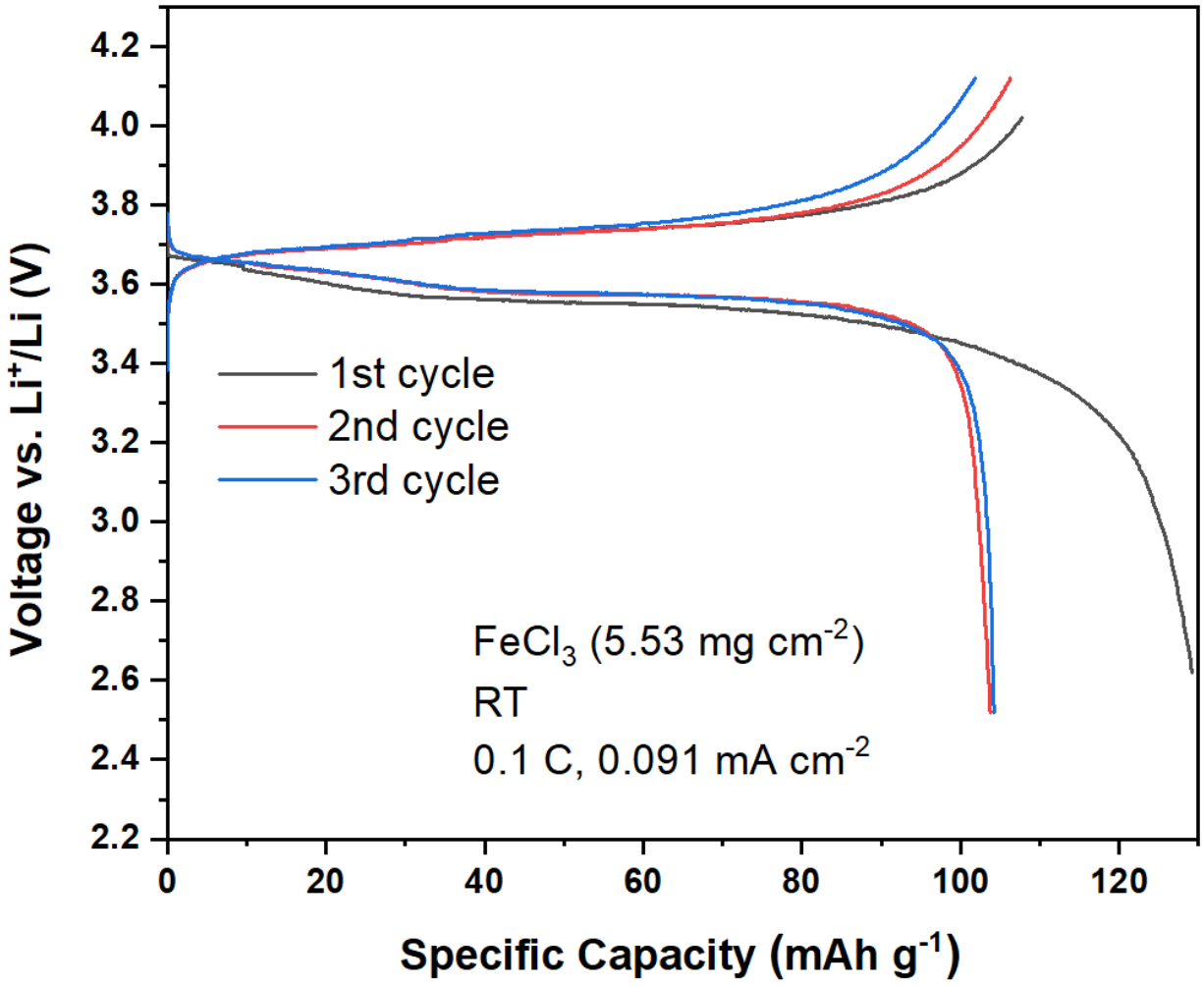

Supplementary Figure 22. Electrochemical performance of $FeCl_3$ cell using Li_2ZrCl_6 electrolytes. The composite cathode has a weight ratio of $FeCl_3$: LZC: C = 70: 27: 3. $Li_3YCl_3Br_3$ (LYCB) is used as a protective layer between LZC electrolyte and In-Li alloy anode.

Supplementary Table 1. Refined structure of discharged $Li_{0.4}FeCl_3$ from XRD data

S.G. $P6_3cm$						
a = 6.2925(47) Å	b = 6.2925(47) Å	c = 23.6252(31) Å	α = β = 90°	γ = 120°		
Site	Wyck.	x	y	Z	Occ.	B_{iso} (Å^2)
Fe1	2a	0	0	0	1.000(0)	0.10(0)
Fe2	4b	0.3333(3)	0.6666(7)	0.2449(6)	0.150(6)	0.10(0)
Fe3	2a	0	0	0.2450(2)	0.749(8)	0.10(0)
Fe4	4b	0.6666(7)	0.3333(3)	0.5	0.540(8)	0.10(0)
Cl1	6c	0	0.6666(7)	0.05464(4)	1	0.50(0)
Cl2	6c	0.3333(3)	0	-0.0300(0)	1	0.50(0)
Cl3	6c	0	0.6666(7)	0.3014(6)	1	0.50(0)
Cl4	6c	0	0.3333(3)	0.1852(1)	1	0.50(0)
Li1	4b	0.25	0.25	0	0.175(3)	2.00(0)

Supplementary Table 2. Refined structure of $Li_{0.8}FeCl_3$ from XRD data

S.G. *C2/m*						
a = 7.2982(14) Å	b = 10.312(2) Å	c = 3.6319(6) Å	β = 89.71°	γ = 90.00°		
Site	Wyck.	x	y	Z	Occ.	B_{iso} (Å^2)
Fe1	2c	0.5	0.5	0.5	1.000(6)	0.10(7)
Cl1	4h	0	0.2407(8)	0.5	1	1.45(8)
Cl2	4i	0.2702(9)	0.5	0	1	1.45(8)
Fe2	4e	0.25	0.25	0	0.175(3)	1.1(3)

Supplementary Table 3. Refined structure of $Li_{0.74}FeCl_3$ from time-of-flight neutron diffraction data

S.G. *C2/m*						
a = 7.2980(12) Å	b = 10.2773(18) Å	c = 3.6219(6) Å	β = 89.695(18)°	γ = 90.00°		
Site	Wyck.	x	y	Z	Occ.	B_{iso} (Å^2)
Fe1	2c	0.5	0.5	0.5	1.000(6)	0.14(5)
Cl1	4h	0	0.2471(3)	0.5	1	0.53(2)
Cl2	4i	0.2768(5)	0.5	0	1	0.53(2)
Fe2	4e	0.25	0.25	0	0.169(2)	0.80(4)
Li1	4e	0.25	0.25	0	0.476(10)	0.80(4)
Li2	4g	0.5	0.125	0	0.024(10)	1.00(80)

Supplementary Table 4. Cost comparison of different cathode/anode pairs.

Battery system	N/P ratio	Average voltage (V)	Cathode capacity (mAh/g)	Cathode cost ($/kWh)	Anode capacity (mAh/g)	Anode cost ($/kWh)	Total cost ($/kWh)
$LiCoO_2$/C	1.05	4.00	160	124.69	370	6.48	131.17
NMC811/C	1.05	3.70	200	81.08	370	7.00	88.08
$LiMn_2O_4$/C	1.05	3.90	120	39.96	370	6.64	46.60
$LiFePO_4$/C	1.05	3.30	170	41.53	370	7.85	49.38
$FeCl_3$/Li	1.05	3.65	165	0.86	3860	2.84	3.70

Note: The cost of Li metal (Li) and graphite (C) are 40 (Alibaba, 2022, https://www.alibaba.com/product-detail/Lithium-metal-99-90-min-with_60565080045.html?spm=a2700.galleryofferlist.normal_offer.d_title.27423b9c9jecy4) and 8.66 $/kg (Beijixing, 2022, https://news.bjx.com.cn/html/20220606/1230755.shtml), respectively.

Supplementary Table 5. Price of chemicals from different vendors used for the estimation in Table S6

Chemical	package size (g)	price per package ($)	unit price ($/kg)
VCl_3 (97%, Sigma)	1	39.20	39200
	5	48.80	9760
	25	171.00	6840
	100	253.00	2530
VCl_3 (97%, Thermal Scientific)	5	46.70	9340
	25	153.00	6120
	100	198.00	1980
VCl_3 (99%, metals basis, Thermal Scientific)	10	103	10300
	50	461	9220
$TiCl_3$-$AlCl_3$ ($TiCl_3$76.0-78.5%, Thermal Scientific)	100	144.97	1449.70
	500	532.81	1065.62
LiCl (anhydrous, 98+%, Sigma)	100	35.60	356.00
	500	75.10	150.20
	2500	216.00	86.40
FeF_2 (anhydrous 98%, Thermal Scientific)	10	101.79	10179.00
	50	270.89	5417.80
$FeCl_3$ (reagent grade 97%, Sigma)	5	46.10	9220.00
	100	53.80	538.00
	1000	72.80	72.80
	2500	130.00	52.00
$FeCl_3$ (anhydrous, 98%, Thermal Scientific)	10	36.30	3630.00
	100	43.90	439.00
	1000	53.70	53.70
	5000	102.00	20.40
	25000	366.00	14.64

Supplementary Table 6. Comparison of energy density and cost of FeF_2, VCl_3, Li_3TiCl_6 and $FeCl_3$

	Theoretical Energy density (Wh/kg)	Estimated raw materials cost * ($/kg)	Cost in $/kWh
VCl_3 (97%, Sigma)	494	15.51	31.39
VCl_3 (97%, Thermal Scientific)		20.72	41.93
VCl_3 (99%, metals basis, Thermal Scientific)		4663.80	9437.89
Li_3TiCl_6 (76.0-78.5%, Thermal Scientific)	362	190.92	527.40
$FeCl_3$ (True market price)	602	0.52	0.86
$FeCl_3$ (reagent 97%, Sigma)		0.24	0.41
$FeCl_3$ (anhydrous, 98%, Thermal Scientific)		0.56	0.92
FeF_2 (98%, Thermal Scientific)	1519	116.31	76.57

* The values of estimated raw materials cost are extrapolated from lab-scale chemical prices listed in Table S5 by using the method by Hart et al. [Cost Eng. 39, 31–35 (1997)]

Supplementary Table 7. Cost analysis of different cathode/anode pairs including electrolytes cost.

Areal capacity (mAh/cm^2)	Areal energy (kWh/m^2)	$FeCl_3$ mass loading (mg/cm^2)	$FeCl_3$ cost ($/m^2$)	Li mass loading (mg/cm^2)	Li cost ($/m^2$)	Li_2ZrCl_6 cost in membrane ($/m^2$)
2	0.07	12.12	0.06	0.54	0.21	0.27
3	0.11	18.18	0.09	0.82	0.31	0.27
4	0.15	24.24	0.13	1.09	0.43	0.27

$FeCl_3$: Li_2ZrCl_6= 55:40					$FeCl_3$: Li_2ZrCl_6= 80:20				
Areal capacity (mAh/cm^2)	**Li_2ZrCl_6 mass loading in cathode (mg/cm^2)**	**Li_2ZrCl_6 cost in cathode ($/m^2$)**	**Total cost ($/m^2$)**	**Total cost ($/kWh)**	**Areal capacity (mAh/cm^2)**	**Li_2ZrCl_6 mass loading in cathode (mg/cm^2)**	**Li_2ZrCl_6 cost in cathode ($/m^2$)**	**Total cost ($/m^2$)**	**Total cost ($/kWh)**
2	8.81	0.97	1.51	21.57	**2**	3.03	0.33	0.87	12.43
3	12.22	1.34	2.01	18.27	**3**	4.5	0.50	1.17	10.64
4	17.63	1.94	2.77	18.47	**4**	6.06	0.67	1.5	10.00

Note: The precursor price of Li_2ZrCl_6 is estimated to be ~ 27 $/L or 11 $/$kg^2$. Freestanding thin SE membrane of 15~20 um can be made via a roll-to-roll process with using a polymer binder[3]. Assuming a porosity of 50% in the solid electrolyte membranes, their cost is estimated to be 0.20~0.27 $/$m^2$.

References

1 Hart, P. W. & Sommerfeld, J. T. Cost estimation of specialty chemicals from laboratory-scale prices: a Publication of the American Association of Cost Engineers. *Cost Engineering* **39**, 31-35 (1997).

2 Kwak, H. *et al.* Emerging Halide Superionic Conductors for All-Solid-State Batteries: Design, Synthesis, and Practical Applications. *ACS Energy Letters* **7**, 1776-1805, doi:10.1021/acsenergylett.2c00438 (2022).

3 Wang, C. *et al.* Solvent-Free Approach for Interweaving Freestanding and Ultrathin Inorganic Solid Electrolyte Membranes. *ACS Energy Letters* **7**, 410-416, doi:10.1021/acsenergylett.1c02261 (2022).